KSME Journal, Vol. 10, No. 4, pp. 423~434, 1996

Impact Damages and Residual Bending Strength of CFRP Composite Laminates Subjected to Impact Loading

Kwang-Hee Im*, Jae-Ki Sim and In-Young Yang*****

(Received January 20, 1996)

The purpose of this study is to confirm the decreasing in residual bending strength, and the failure mechanisms experimentally when CFRP composite laminates are subjected to foreign object damage(FOD). Composite laminates used in this test are CFRP orthotropic laminated plates, which are stacked with two-interfaces $[0°_6/90°_6]_{sym}$ and four-interfaces $[0°_3/90°_6/0°_3]_{sym}$. When the specimen was subjected to transverse impact by a steel ball, the delamination area generated by the impact damage was observed by using the SAM(scanning acoustic microscope). Also, the fracture surfaces obtained by three-point bending test were observed by using the SEM(scanning electron microscope). Further, failure mechanisms were investigated based on the observed delamination areas and fracture surfaces.

Key Words: Foreign Object Damage, Impact Damage, CFRP, Delamination Area, Impact Energy, Residual Bending Strength

1. Introduction

Currently, carbon-fiber reinforced plastics (CFRP) are widely used in both space and civil aircraft due to their superior stiffness and strength to weight ratios compared to conventional metallic materials.

Unfortunately, CFRP laminates are brittle for dynamic loading, particularly impact loading(Tanaka, 1989), which can significantly reduce their properties; so the impact problems of composites are becoming important. A dropped wrench, bird strike (Ma, 1991) or runway debris can generate localized delaminated areas of foreign object damage(FOD) (Takeda, 1985) by an impact which are frequently difficult to detect using the naked eyes.

* Graduate Student, Department of Mechanical Engineering Chosun University 375 Sosok-dong, Dong-gu Kwangju 501-759, Korea

** Department of Precision Mechanical Engineering Chosun University 375 Sosok-dong, Dong-gu Kwangju 501-759, Korea

*** Department of Mechanical Design Engineering Chosun University 375 Sosok-dong, Dong-gu Kwangju 501-759, Korea

Innocuous though this damage may seem in the stacking plates, it can result in premature catastrophic failure due to the decreasing strength caused by impact loading. When the laminates are subjected to a transverse impact load, the fracture bending strength decrease noticeably(Greszczuk, 1977 ; Challenger, 1986 ; Ishai, 1990). For this reason, Rotem(Rotem, 1988) and Kurokawa (Tanaka, 1989) have recently studied the decreasing relationship experimently by using a three-point and four-point bending test. However, their works have shown only the relationship between impact energy and delamination areas or residual strength decrease. They did not present a failure mechanism of residual strength decreased by impact damage.

Therefore, the interrelations between impact energy and delamination damage areas and impact energy vs. critical delamination energy were investigated when the orthotropic laminates, stacked with the same number of plies but different stacking configurations, were subjected to impact loads.

This paper attempts to evaluate the decreasing relationship of the residual bending strength of the laminates through the three-point bending

Table 1 Characteristics of CF/EFOXY specimen

Characteristics \ Type	Carbon fiber	Resin	Prepreg
Maker	JapanTORAY	JapanTORAY	
Model	T300-3000	#2500	P. 3051-15
Density	1.75×10^3[kg/m^3]	1.24×10^3[kg/m^3]	
Tension strength	3530[MPa]	78[MPa]	
Elastic modulus	230[GPa]	3.96[GPa]	
Elongation	1.5[%]	2.0[%]	
Resin content			37[% WT]

test, and to confirm the failure mechanisms.

2. Experimental Method

2.1 Specimen configurations

The laminates of the specimens were manufactured from one-directional prepreg sheets of T300-3000 carbon fibers and #2500 epoxy resin in Japan Toray P3051-15, cured to the manufacturer's specifications. Two types of specimens were used in this experimentation. Their lay-up, stacked with 24 plies, indicates that specimen A is $[0°_6/90°_6]_{sym}$. and specimen B is $[0°_3/90°_6/0°_3]_{sym}$.. Test specimens were prepared with dimensions 40mm × 180mm × 3.75mm (width × length × thickness). The fiber-direction of specimen surface was manufactured to correspond to 0° direction; in order that, the fiber-direction is the same as the the length direction. By regulating the width of unimpacted specimens larger than that of specimens generated by an impact load, it is possible that none of the results of experimentation are influenced by the edge effects. By properly mainpulating the harding temperature point with the use of the heater at the vacuum bag of autoclave, the CFRP laminates can be cured. After laminating the prepreges of the desired direction, the inner temperature was heated up to 200℃ which was measured by using a thermcouple. The temperature was controlled by a controller. After holding the vacuuming condition of the vacuum bag up tp 10^{-1}pa in forming. the pressure of 5×10^5 pa is added to the vacuum bag from the outer side of the bag by using the compressor.

Fig. 1 Photo of impact test apparatus

2.2 Impact experiments

The test fixture consisted of two steel plates(10 mm in thickness) and two rubber plates(10 mm in thickness), which were cut in the form of a circular hole(150mm diameter) at the center of plates, and the specimen was supported in the space between the rubber plates with the steel plates on each side. A steel ball 5mm in diameter (0.5g) was impacted on the specimen by using compressed air as shown in Fig. 1.

The velocity of the steel ball was measured just before impact by determining the time taken for it to pass two fine laser beams located a known distance(10mm) apart. The impact velocity was obtained by varying air pressures on a compresser. The impact energy was 1.7J(with a velocity of 82.64m/s) and 2.5J(with a velocity of 100 m/s). The impact energy shows just the kinetic energy of the impactor prior to impact.

Fig. 2 Photo of ultransonic microscope

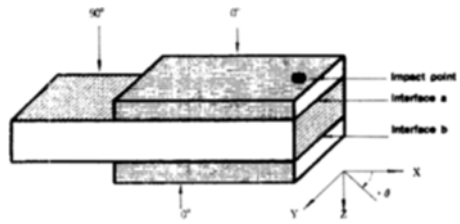

(a) Specimen A

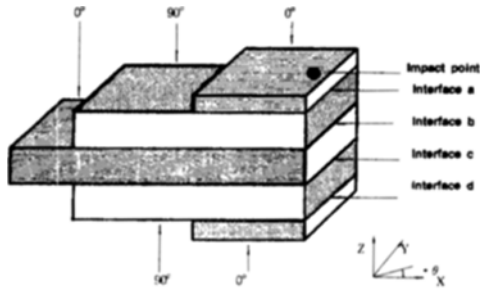

(b) Specimen B

Fig. 3 Schematic representation of laminate orientation code and interfaces for CFRP Specimen interfaces of CFRP Specimen

2.3 Damage detection techniques

After impact, the delamination of specimen interfaces was assessed using an ultrasonic microscope(Olympus UH100 with the range of 30 MHz). Simply, after labeling each interface a, b, c, and d from the impact point shown in Fig. 3, interface a on the impacted side was observed in the case of specimen A, and interface b on the opposite impacted side was observed, and the total delamination area of each was measured.

The measuring methods for the delamination areas are as follows; each interface is classified according to colors, the distributed range of each color is measured using the ultrasonic microscope, and the total delamination area is obtained by adding up all delamination areas. In the case of specimen B, we observed the interfaces a and b from the impact side, and then observed the interfaces c and d on the opposite impacted side because of there being four interfaces. Also, interface a causes a section of interface b to be invisible, and interface d causes a section of interface c partly to be invisible. For this reason, we measured delamination areas as projection areas due to the characteristics of the ultrasonic microscope. The ultrasonics of frequency such as a high -frequency volt is sent to the piezo transducers on the acoustic lens and the ultrasonics can be convergent due to the spherical section of acoustic lens. In order to magnify the medium from the lens, water greater than density of air is used as the medium.

2.4 Static three-point bending test

To examine residual bending strength of the specimen subjected to impact damages, a static three-point bending test was carried out. Figure 4(a) shows the fixture attached to the universal testing machine(Instron 8501) for the experiments of impacted-side tension and impacted -side compression.

In the bending test, the maximum loading and bending stresses were measured when the specimen was fractured. And the fracture surfaces were examined using a JSM-T200 scanning electron microscope(SEM) with a magnification of between 35 and 100,000 times.

The fracture bending stresses were measured on the assumption that the specimen were homogeneous isotropic materials(Malvern, 1989) because the stresses of CFRP laminates are linearly proportional to strain up to the point of rupture. The effects of dimension error can be eliminated by using a ture measurment(i. e. at a width and thickness of a specimen).

The fracture bending stress equations are as follows:

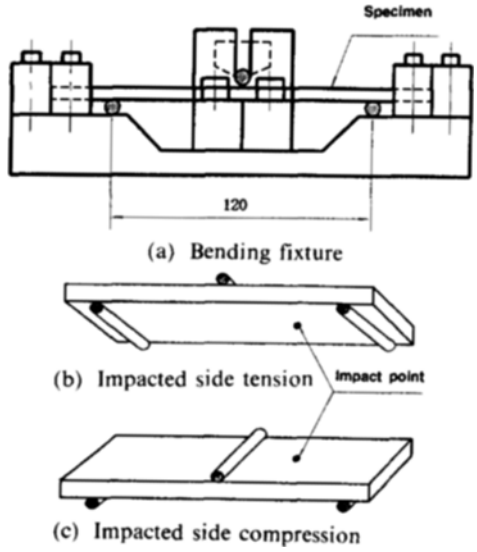

Fig. 4 Specimen supporting fixture of 3-Point test

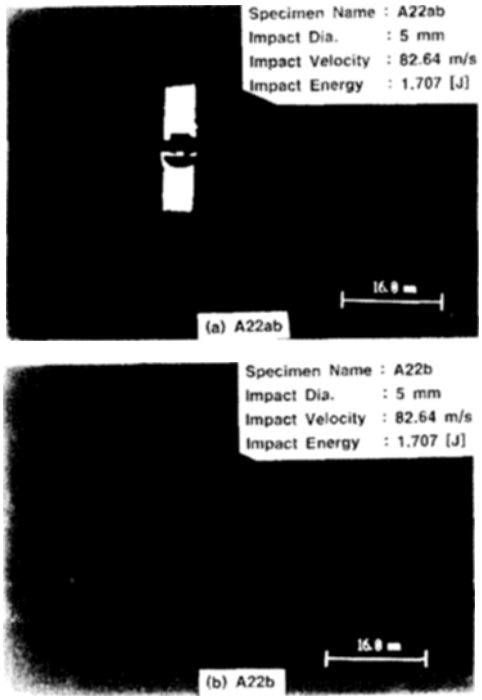

Fig. 5 Delamination areas of specimen A

$$I=\frac{bd^3}{12}$$

$$\sigma=\frac{(PL/4)(d/2)}{I}=\frac{3PL}{2bd^2} \quad (1)$$

where σ is the bending stress(Pa), P is the maximum loading at fracture(N), L is the length of span(m), b is the width of specimen(m), d is the thickness of specimen(m), and I is the moment of inertia(m^4).

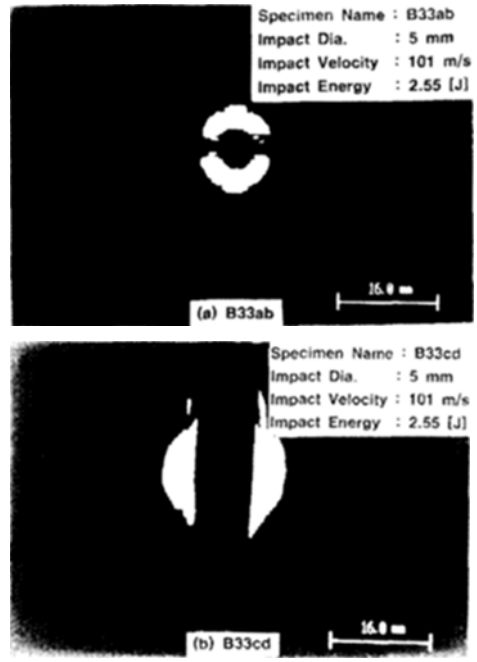

Fig. 6 Delamination areas of specimen B

3. Discussion

3.1 Relation between impact energy and delamination areas

When the specimen of CFRP is subjected to impact loading, Figs. 5~6 show the areas of damage delamination, which was photographed by the SAM. Figure 5(a) shows the synthesized photo, which indicates the delamination areas of interfaces a and b for specimen A, red indicates interface a, and green indicates interface b. Figure 5(b) shows the delamination areas of interface b for specimen A. Figure 6(a) shows the delamination areas of interfaces a and b at the impacted side, photographed from specimen B with four interfaces, red indicates interface a, and green indicates interface b. Figure 6(b) shows the delamination areas of interfaces c and d at the opposite-impacted side, photographed from specimen B, blue indicates interface c, and red indiactes interface d.

The specimen rules are assumed as follows:

Table 2 Results of delamination area measurment and three-point bending test

Names of specimen	Impact test							3-Point bending test	
	Impact velocity (m/s)	Impact energy (J)	Delamination areas (mm^2)				Total	Conditions of bending test	Stress of fracture bending(GPa)
			Inter.a	Inter.b	Inter.c	Inter.d			
AN1	0	0					0		1.493
AN2	0	0					0		1.570
A20	29.50	0.61	10.06	15.00			25.06		
A21	82.64	1.707	110.13	453.00			563.17	I. S. C.	0.789
A22	82.64	1.707	77.60	399.29			477.00		
A23	82.00	1.680	132.70	449.67			582.37	I. S. T.	0.862
A24	82.64	1.707	93.60	390.00			483.6	I. S. C.	0.890
A25	82.64	1.707	94.20	384.80			479.00	I. S. T.	0.957
A26	82.64	1.707	93.10	388.40			481.50		
A31	95.24	2.267	128.26	553.82			682.08		
A27	90.20	2.034	101.20	399.20			500.40		
A32	102.00	2.601	139.67	678.64			818.31		
A33	101.00	2.550	130.43	630.17			760.60	I. S. T.	0.792
A34	100.00	2.550	130.43	613.75			750.00	I. S. C.	0.757
A35	102	2.601						I. S. T.	0.769
A36	101	2.550						I. S. C.	0.661
BN1	0	0					0		1.111
BN2	0	0					0		1.120
B21	82.64	1.707	36.60	37.730	93.55	0	167.88	I. S. C.	0.983
B22	82.64	1.707	37.12	42.95	84.67	11.06	175.80		
B23	82.00	1.680	33.48	32.51	97.15	10.20	173.34	I. S. T.	1.114
B31	94.30	2.223	59.67	40.31	115.75	41.60	257.33	I. S. C.	0.843
B32	100.00	2.500	45.95	42.56	198.40	61.31	348.28	I. S. T.	0.994
B33	101.00	2.550	66.14	63.86	208.10	93.90	432.00		

* I. S. T. : impacted-side tension, I. S. C. : impacted-side compression

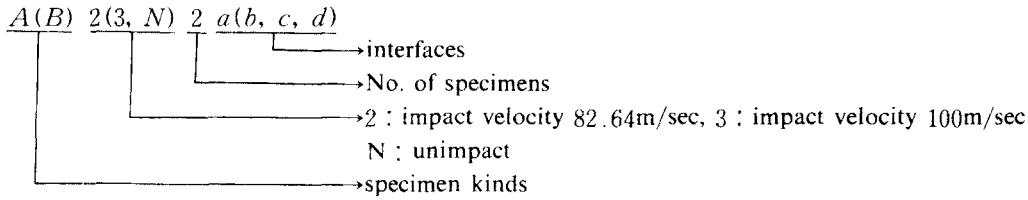

Results of delamination area measurement and the three-point bending test are shown in Table 1.

In Fig. 7, a solid line is interpolated by the method of least squares, and specimens A and B show a linear relation. With an increase of the specimen interfaces, the impact energy was increased, which caused an initial delamination, the critical delamination energy of specimen B with four interfaces is about 0.860 J, the critical delamination energy of specimen A with two interfaces is about 0.410 J; it was found that the critical delamination energy of specimen B is about 2 times greater than that of specimen A. Therfore, the impact damages of the specimens with more interfaces are less because the critical delamination energy is greater. With an increase

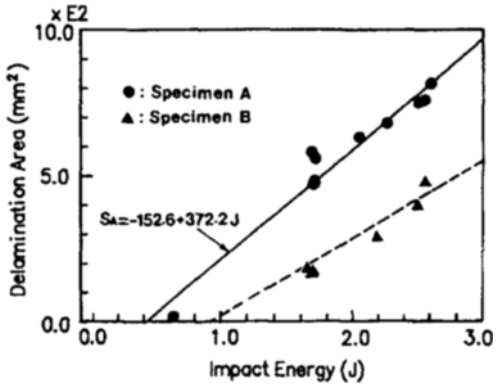

Fig. 7 Relation between impact energy and delamination areas of specimens A and B

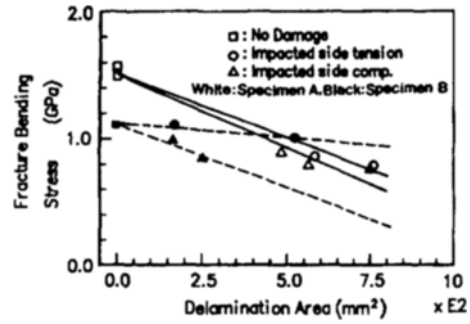

Fig. 8 Relation between delamination area and fracture bending stress of specimens A and B

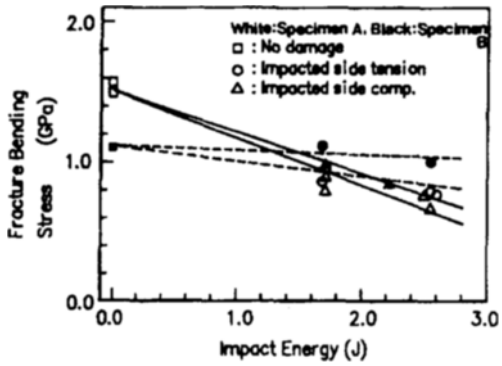

Fig. 9 Relation between impact energy and fracture bending stress of specimens A and B

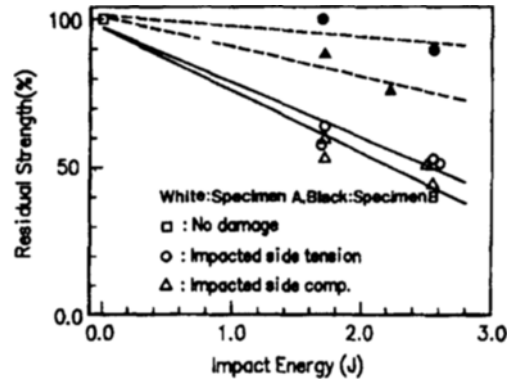

Fig. 10 Relation between impact energy and residual strength of specimens A and B

in the specimen interfaces shown in Fig. 7, the delamination area per unit impact energy(mm^2/J) is decreased, which shows the magnitude of delamination areas S_A and S_B(mm^2) according to the magnitude of impact energy. From the above relations, it is found that the impact damage rate over impact energy of the laminates with more interfaces appears less than that of the laminates with less interfaces.

3.2 Results of the static three-point bending test

After observing the interface damage range of the specimens with impact damage by the SAM, the static three-point bending test was performed to consider the decreasing relation of residual bending strength.

Figure 8 shows the relation between delamina-

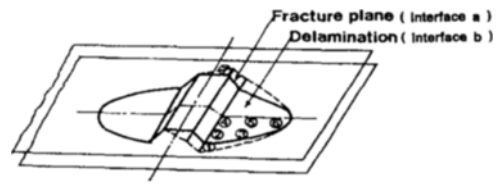

(a) Impacted side compression

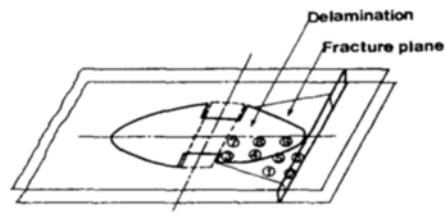

(b) Impacted side tension

Fig. 11 Observation point of fracture and delamination surface

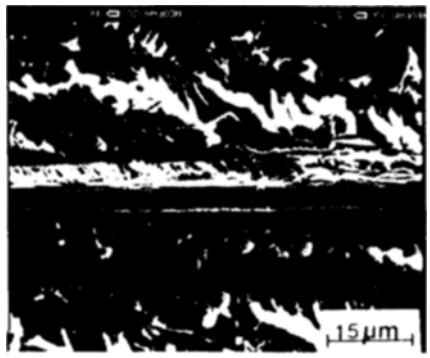

Point④

Point⑤

Point⑥

Fig. 12 Fractography of delamination and fracture surface (Impacted-side compression) (magnification 500×)

tion areas and fracture bending stresses of specimens A and B for each case of impacted-side tension and impacted-side compression; also

Point⑦

Figure 9 shows the relation between impact energy and fracture bending stresses of specimens A and B for each case. Figure 10 shows the relation between impact energy and residual bending strength of specmens A and B, and when the fracture bending strength ratio of unimpacted specimens is assumed to be 100%, the ratio of residual strength is the ratio of the impacted specimen to the unimpacted specimen. From these results obtained above, the decreasing phenomena of residual strength appear higher for impacted side compression than for impacted side tension over each specimen (A and B). Figure 8 reveals that with an increase of delamination areas for specimen A, the strength of impacted-side compression decreases a little over that of impacted -side tension. Also, in the case of specimen B stacked with more interfaces, we can find radically decreasing phenomena.

Figure 9 shows a higher strength of approximately 38% more for specimen A stacked with less interfaces than for specimen B stacked with more interfaces in the case of unimpact. Also, within the range of impact energy 1.45 J for impacted -side tension, and of impact energy 1.65 J for impacted-side compression when subjected to impact damages, the impact resistance appears higher for specimen A stacked with two interfaces than for specimen B stacked with four interfaces. On the other hand, residual bending strength of specimen A is greater than that of specimen B within the impact range of impact energy 1.65 J (impacted-side compression) and 1.45 J (impacted-side tension), and residual bending

Point①

Point②

Point③

(**Fig. 12** continued)

strength of specimen A is smaller than that of specimen B.

For the above impact range, the residual bending strength appears less for specimen A than for specimen B. Therfore, in the case of specimens stacked with less interfaces, the residual strength radically decreases due to impact damages over the case of specimens stacked with more interfaces. Therefore, in the case of specimen A in which the residual strength radically decreases, we consider the failure mechanism through observing the fracture surface by the SEM.

3.3 Failure mechanism

As described in Sec. 3.2, to examine the decreasing phenomena of radically residual strength for specimen A impact damages, the static three-point bending test was conducted, and then, the damaged specimen surface was observed using the SEM for each case of impacted-side compression and impacted-side tension of specimen A subjected to impact damages.

To observe the fracture growth direction and the interface delamination of CFRP laminates at each interface under the impact damages, the SEM was used by removing separate interfaces with a dimaond cutter from a damaged specimen for more detailed examination of the failure mechanisms. In order not to remove the internal delamination areas, a specimen for surface-observation was prepared with the spattering on the fracture surface and delamination surface.

Figure 11 shows the observation positions of fracture and delamination surface, only a quarter section, due to the delamintion areas symmetrically formed from the impact point. Figure 12 shows the fractography of delamination and the fracture surface for interface b with impacted side compression. Figure 13 shows the fractography of the delamination and the fracture surface for interface b with impacted-side tension. From the photo, it is clear that the fracture impacted-side compression grew at the transverse cracks, which occured at an impact point by total delamination of interface b(90/0°) under tension. From the hackle direction(Smith, 1987) showing the resin shapes, which is generated by a shear failure, the shear direction can easily be found, but in the case of impacted-side compression shown in Fig. 12, the hackle direction reveals that the delamination growth direction in the middle of the delamination surface(see points 4, 5, and 6 in Fig. 11(a)) is directed to the 0°-direction delamina-

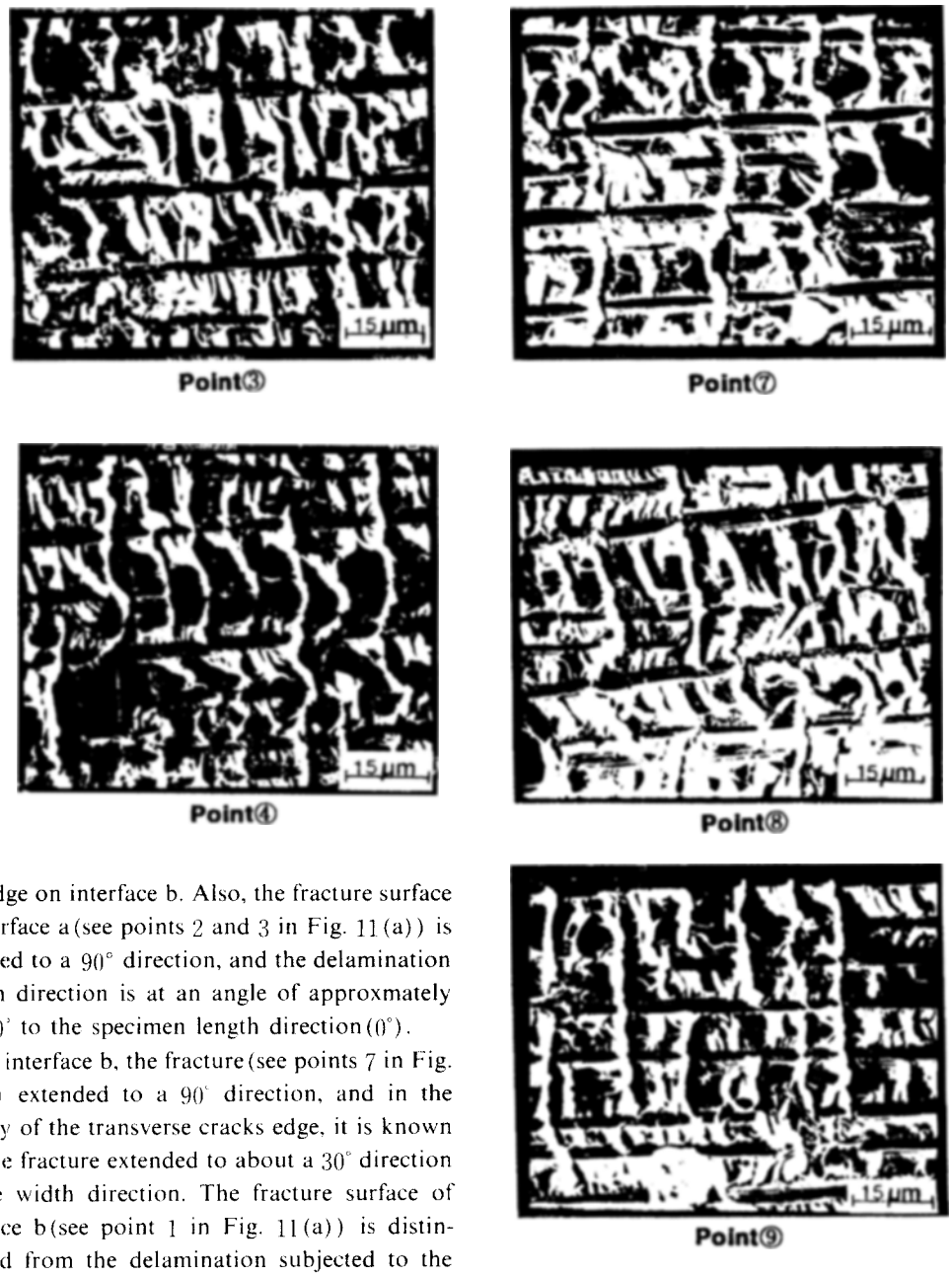

Fig. 13 Fractography of delamination and fracture surface (Impacted-side tension) (magnification 500×)

tion edge on interface b. Also, the fracture surface of interface a (see points 2 and 3 in Fig. 11(a)) is extended to a 90° direction, and the delamination growth direction is at an angle of approxmately 20~30° to the specimen length direction (0°).

For interface b, the fracture (see points 7 in Fig. 11(a)) extended to a 90° direction, and in the vicinity of the transverse cracks edge, it is known that the fracture extended to about a 30° direction by the width direction. The fracture surface of interface b (see point 1 in Fig. 11(a)) is distinguished from the delamination subjected to the impact damages, but it is found that the fracture extended in the same delamination direction.

In the case of impacted-side tension, the transverse cracks occured at the delamination edge of interface b, and extended to the impact point along interface b. In the case of impacted-side tension shown in Fig. 13, the hackle direction reveals that the delamination had grown to the 0° direction such as shown on the delamination surface of interface b (see points 3, 4, 7, 8, and 9 in Fig. 11(b)) for impacted-side tension.

But, contrary to impacted-side compression, it is known that the specimen fractures (see points 1, 2, 5, and 6 in Fig. 11(b)) grew from the trans-

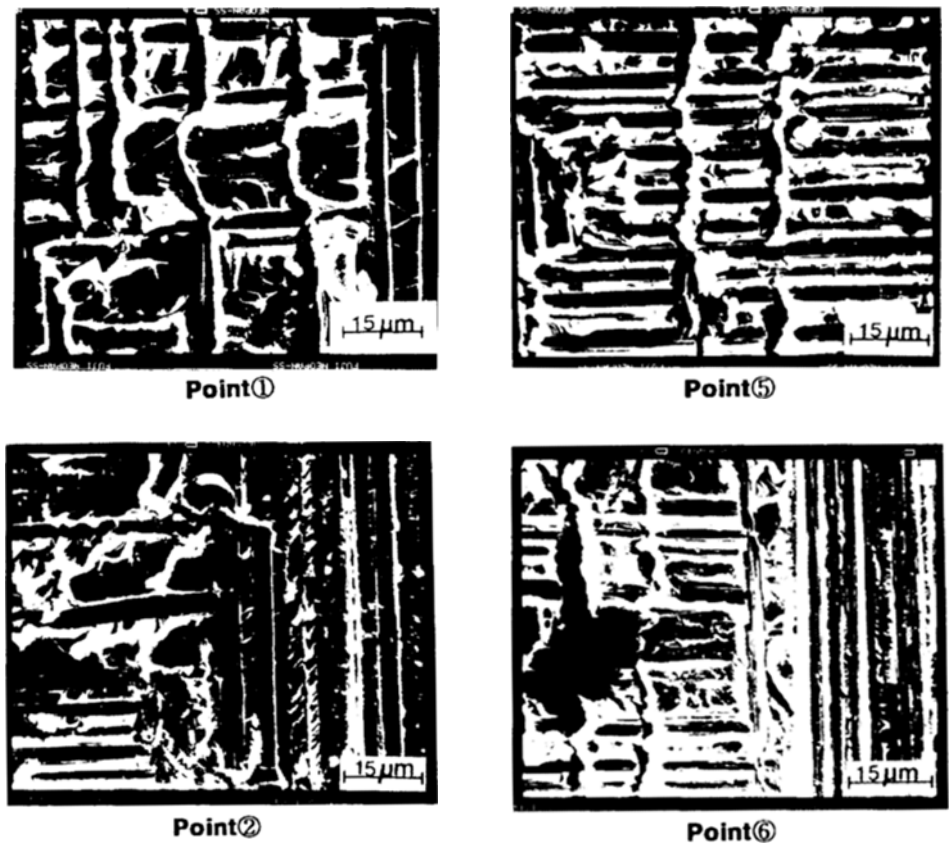

(**Fig. 13** continued)

verse cracks generated at the delamination edge of interface b toward the impact point.

Figures. 14 and 15 show the fracture modes by conducting the three-point bending test, using the specimens which were subjected to impact damages, and show the delamination growth direction from the fracture surface photo of Figs. 12 and 13. In the case of impacted-side compression shown in Fig. 14(a), the delaminations of interfaces a and b grew along the transverseracks generated below the impact point, and the delamination possessing the greatest growth width was the delamination for interface b on the tension side.

To explain the phenomena, Fig. 14(a) shows in detail the fracture growth modes in consideration of shear stresses, tension and compression in the plane. When the transverse cracks extend in the tension direction in these modes, the opening displacement becomes greater, and when the cracks extend in the compression direction, the closing phenomena occur on the contrary.

Thus, because the opening displacements on the tension side(modes I + II) are higher than those on the compressure side, delamination on the tension side can easily be extended. Therfore, when the delamination develops in each ply, the interface modes can be assumed as shown in Figure 14(a). The cause of transverse cracks occuring from impact loading reveals that the delaminations grew from the shearing strain generated during the three-point bending test. Figure 14(b) shows the delamination, and fracture surface growth direction. Also, in the case of impacted-side tension shown in Fig. 15(a), transverse cracks, which are at the delamination edge of interface b on the compression side, occur, and it is known that the delamination of interface b

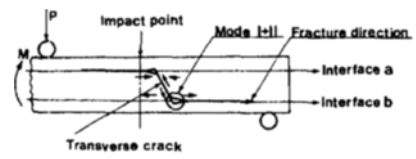

(a) Damage develement mode

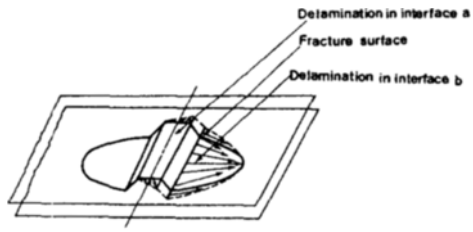

(b) Fracture develement direction

Fig. 14 Diagram of failure mechanisms (Impacted-side compression)

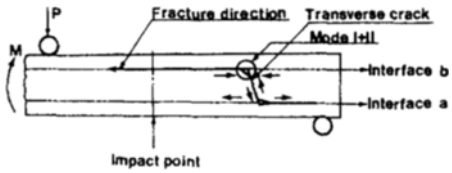

(a) Damage develement mode

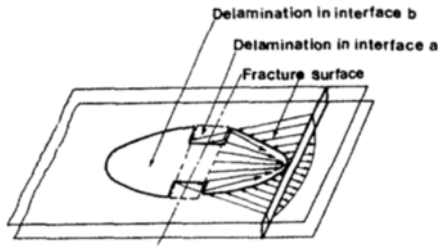

(b) Fracture develement direction

Fig. 15 Diagram of failure mechanisms (Impacted-side tension)

grew toward the impact point. To explain these phenomena, Fig. 15(a) shows in detail the fracture growth modes in consideration of shear stresses, tension and compression in the plane. When the transverse cracks develope in the compression direction for the modes (modes I + II), the opening displacement in interface b becomes greater, and then, delamination grew.

Therefore, the delamination and the growth direction of the fracture surface can be assumed as shown in Fig. 15(a), and delamination growth by shear strain causes each interface to fail. Figure 15(b) shows the delamination and the growth direction of the fracture surface. Thus, as shown in Figs. 14 and 15, the moment becomes greater because the radius of curvature at the fracture starting point was smaller in the case of impacted-side tension than in the case of impacted-side compression from the impact point. So, it is thought that more fractures develop immediately under impacted-side compression than under impacted-side tension.

Also, the CFRP laminates subjected to impact damages are weaker under compressure than under tension on the shock resistant.

In addition, the fractured fibers generated by the impact damages at the impact point depend upon the residual compression strength compared to the residual tension strength. From the results of all the methods discussed, it is clear that fractures develop more in the case of impacted-side compression than in the case of impacted-side tension for the BAI(bending strength after impact) test of the laminates subjected to impact damages.

4. Conclusions

After impacting on the CFRP laminates, the delamination areas were observed, residual strength was evaluated, and the failure mechanisms and the decreasing in residual strength were analyzed.

The following conclusions can be made within the range of this observation:

(1) It has been found that for the specimen with more interfaces, critical delamination energy is increased while delamination-developement energy is decreased.

(2) The residual bending strength of specimen A is greater than that of specimen B within the impact range of impact energy 1.65J (impacted

-side compression) and 1.45J (impacted-side tension). On the other hand, when the impact energy is beyond the above ranges, the residual bending strength of specimen A is smaller than that of specimen B.

(3) In specimens A and B, the residual strength of CFRP plates subjected to impact damages is higher for impacted-side compression than for impacted-side tension.

(4) In the case of impacted-side compression, the fracture is initiated at the transverse cracks generated near the impact point. On the other hand, the fracture grew to the impact point from the edge of interface-b delamination in the case of impacted-side tension.

Acknowledgments

This study was supported by Factory Automation Center for Parts of Vehicles (FACPOV) in Chosun University, Kwangju, Korea. FACPOV is designated as a regional research center of Korea Science and Engineering Foundation (KOSEF) and operated by Chosun University.

References

Challenger, K. D., 1986, "The Damage Tolerance of Carbon Fiber Reinforced Composites"-A Workshop Summary, Composite Struct., pp. 295~318.

Greszczuk, L. B. and Chao, H., 1977, "Impact Damage in Graphite-Fiber-Reinforced Composites," *ASTM STP* 617, ASTM. Philadelphia, pp. 389~408.

Ishai, O. and Shragi, A., 1990, "Effect of Impact Loading on Damage and Residual Compressive Strength of CFRP Laminated Beams,", *Composite Struct.*, 14-4, pp. 319~337.

Ma, C. C. M., Huang, Y. H., and Chang, M. J., 1991, "Hygrothermal Effect on the PEEK/C. F. and PPS/C. F. under Impact Loading(I)," *ANTEC*, pp. 2029~2096.

Malvern, L. E., Sun, C. T. and Liu, D., 1989, "Delamination Damage in Central Impacts at Subperformation Speeds on Laminated Kevlar/Epoxy Plates," *ASTM. STP*. 1012, pp. 387~405.

Rotem, A., 1988, "Residual Flexural Strength of FRP Composite Specimens Subjected to Transverse Impact Loading," *SAMPE Journal*, pp. 19~25.

Smith, B. W. and Grove, R. A., 1987, "Determination of Crack Propagation Directions in Graphite/Epoxy Structures," *Composites and Metals, ASTM. STP*. 948, pp. 154~173.

Takeda, T., 1985, "Impulsive Response and Fracture of Composites(I)," *Journal of the Japan Society for Composite Materials*, Vol. 11, No. 4, pp. 151~161.

Tanaka, T., Kurokawa, T., etc., 1989, "Damage and Residual Bending Strength of Graphite/Epoxy Composite Laminates Subjected to Normal Impact," *Journal of the Japan Society for Aeronautical & Space Sciences*, Vol. 37, No. 25, pp. 29~36.